Available online at www.sciencedirect.com

ScienceDirect

Procedia Structural Integrity 2 (2016) 1359–1366

Structural Integrity Procedia

www.elsevier.com/locate/procedia

21st European Conference on Fracture, ECF21, 20-24 June 2016, Catania, Italy

Fatigue crack propagation properties of submicron-thick freestanding copper films in vacuum environment

Toshiyuki KONDO[a,*], Akihiro SHIN[a], Hiroyuki HIRAKATA[a] and Kohji MINOSHIMA[a]

[a]*Department of Mechanical Engineering, Osaka University, 2-1 Yamadaoka, Suita, Osaka 565-0871, Japan*

Abstract

Fatigue crack propagation experiments were conducted in approximately 500 nm thick freestanding copper (Cu) films in both air and vacuum environments to clarify the effects of vacuum environment on fatigue crack propagation properties. First, we newly developed an experimental setup for fatigue crack propagation experiments of the freestanding Cu films inside a vacuum chamber of a field-emission scanning electron microscope (FESEM). Fatigue crack propagation experiments were conducted in ambient air and vacuum environment of the FESEM chamber (~10^{-4} Pa) under load-control conditions with constant maximum stress and at a stress ratio R of 0.1. *In situ* FESEM observations of fatigue crack propagation confirmed that preceding intrusions/extrusions were formed ahead of the fatigue crack tip, and the fatigue crack then propagated preferentially through these intrusions/extrusions in the lower stress intensity factor range (ΔK). In the higher ΔK, the fatigue crack propagated in tensile fracture mode. These mechanisms of fatigue crack propagation were similar to those in air. The relationships between fatigue crack propagation rate (da/dN) and stress intensity factor range (ΔK) in both environments were roughly within a narrow band in the region of $\Delta K \gtrsim$ 4–5 MPam$^{1/2}$. On the other hand, da/dN in vacuum became smaller than that in air in the region of $\Delta K \lesssim$ 4–5 MPam$^{1/2}$. FESEM observations confirmed that the fracture surfaces morphologies depended on the environments in $\Delta K \lesssim$ 4–5 MPam$^{1/2}$: flat fracture surface were mainly observed in air, whereas, in vacuum environment, blunt fracture surface with fine roughness were mainly observed. This suggests that reversible cyclic slip deformation and rewelding occurred in vacuum environments, resulting in smaller da/dN in vacuum than air.

Peer-review under responsibility of the Scientific Committee of ECF21.

Keywords: fatigue; crack propagation; thin films; environmental effects; copper

* Corresponding author. Tel.: +81-6-6879-7242; fax: +81-6-6879-7243.
E-mail address: kondo@mech.eng.osaka-u.ac.jp

Copyright © 2016 The Authors. Published by Elsevier B.V. This is an open access article under the CC BY-NC-ND license (http://creativecommons.org/licenses/by-nc-nd/4.0/).
Peer review under responsibility of the Scientific Committee of ECF21.
10.1016/j.prostr.2016.06.173

1. Introduction

In bulk metals, effects of vacuum environment were observed on fatigue crack propagation properties. Because fresh surface oxidation is suppressed in vacuum environments, cyclic slip deformation at the crack tip becomes reversible during loading and unloading process (Pelloux (1970)). In addition, fresh fracture surfaces behind the crack tip can reweld together (Hudson and Seward (1976)). In contrast, the surface oxide layer was formed on the fresh surface in the slip deformation at the crack tip in air, resulting that cyclic slip deformation at the crack tip becomes irreversible compared in vacuum environment. Moreover, rewelding of fracture surfaces becomes difficult because of the presence of oxide layer. Hence, accumulation of fatigue damage at the crack tip in vacuum is smaller than that in air, leading to smaller da/dN in vacuum than air (Ishii, Weertman (1969)).

Kondo et al. (2013) conducted fatigue crack propagation experiments in approximately 500 nm thick freestanding copper (Cu) films in ambient air at a stress ratio R of 0.1, 0.5 and 0.8. In a high-K_{max} region (maximum stress intensity factor $K_{max} \geq 4.5$ MPam$^{1/2}$), the fatigue crack propagated by tensile fracture mode, and the fracture surface showed chisel-point fracture regardless of R. In a low-K_{max} region ($K_{max} < 4.5$ MPam$^{1/2}$), preceding intrusions/extrusions were formed ahead of the fatigue crack, and the fatigue crack then propagated preferentially through these intrusions/extrusions. These fatigue crack propagation mechanisms were different from those in bulk metals. Hence, the effects of vacuum environments on fatigue crack propagation properties in submicron-thick freestanding metallic films would be different from those in bulk metals.

The purpose of this study is to clarify the effects of vacuum environment on fatigue crack propagation properties of submicron-thick freestanding metallic films. First, we newly developed an experimental setup for fatigue crack propagation experiments of submicron-thick freestanding metallic films in both air and vacuum environments. Fatigue crack propagation experiments in approximately 500 nm thick freestanding Cu films were conducted in both air and vacuum environments. On the basis of the comparison of fatigue crack propagation behavior and fracture surface morphologies, the effects of vacuum environment on fatigue crack propagation properties of submicron-thick freestanding Cu films are discussed.

Nomenclature

a	Crack length
B	Film thickness
da/dN	Fatigue crack propagation rate
ΔK	Stress intensity factor range (= $K_{max} - K_{min}$)
f	Frequency
K	Stress intensity factor
K_{max}	Maximum stress intensity factor
K_{min}	Minimum stress intensity factor
N	Number of cycles
R	Stress ratio (K_{min}/K_{max})
σ_{max}	Maximum stress
σ	Nominal stress
W	Specimen width

2. Experimental

2.1. Materials and specimens

The tested materials were Cu films with a film thickness (B) of 523 nm, deposited by electron beam evaporation method. The purity of the Cu evaporant was 99.999%. Figure 1 shows a crystal orientation map of the film taken by electron backscatter diffraction (EBSD) analysis (EDAX Inc., DigiView). Black lines indicate the grain boundaries.

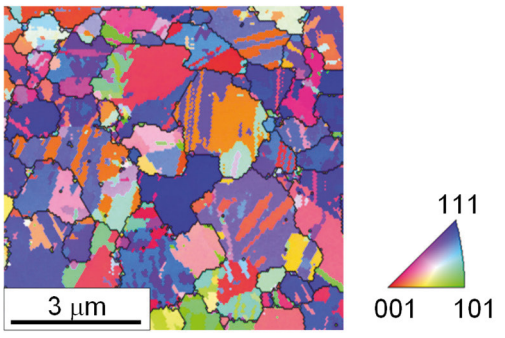

Fig. 1 Crystal orientation map of approximately 500 nm thick Cu film.

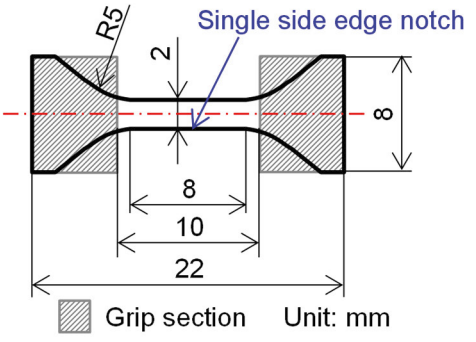

Fig. 2 Shape and dimensions of the freestanding film specimen.

Σ3 twin boundaries were observed inside the grains. Average grain size considering and not considering twin boundaries as grain boundaries were roughly 250 nm and 660 nm, respectively.

Figure 2 shows the shape and dimensions of a specimen. Freestanding film specimens were fabricated by the sacrificial layer wet etching method (Kondo et al. (2013)). A single side edge notch with a length of roughly 100 μm was introduced to the gage section of the film specimen by using the focused ion bean system (FEI Company, Versa 3D).

2.2. Experimental setup and test conditions

An *in situ* FESEM fatigue testing machine for freestanding film specimens was newly developed in-house. Figure 3 shows the external appearance of the fatigue testing machine. This machine is able to conduct fatigue crack propagation experiments in a freestanding film specimen inside a vacuum chamber of an FESEM (FEI Company, Versa 3D). To apply high frequency cyclic load to the freestanding film specimen, the displacement of a piezoelectric actuator (Piezomechanik GmbH, PSt 150/7/100 VS12, maximum stroke: 100 μm, precision: ±0.02 μm) was transferred by the specimen jig attached to the linear guide frame. The load cell for small load (Kyowa Electronic Instruments Co., Ltd., LTS-50GA, rated capacity: 500 mN, precision: ±0.11 mN) was employed to measure applied cyclic load. Because the displacement of the piezoelectric actuator is small (maximum stroke: 100 μm), a long-stroke positioning stage incorporating piezo actuator (Newport Corporation, Picomotor piezo linear actuator 8310-V, maximum stroke: 12.7 mm, precision: ±0.061 μm) was employed adjunctively for positioning.

Fatigue crack propagation experiments were conducted at R of 0.1. Cyclic stress with a sinusoidal waveform was applied at a frequency f of 10 Hz and the maximum stress (σ_{max}) was held at 130 MPa. K was calculated from the equation for a single side edge crack in a finite-width body (Murakami (1986)).

$$K = \sigma\sqrt{\pi a}F(\alpha) \tag{1}$$
$$F(\alpha) = 1.12 - 0.231\alpha + 10.55\alpha^2 - 21.72\alpha^3 + 30.39\alpha^4$$
$$\alpha = \frac{a}{W}$$

Here, σ denotes the nominal stress, W is the specimen width (2 mm) and a is the crack length. Crack length a was measured on the basis of the observed FESEM images in vacuum and the observed optical microscope images in air.

Fatigue crack propagation experiment in air was conducted in ambient air with room temperature of 298±5 K and relative humidity of 30–60%. The experiment in vacuum was conducted inside the FESEM with chamber pressure of ~6.3×10^{-4} Pa. *In situ* FESEM observation was conducted while holding a constant tensile stress at $0.8\sigma_{max}$ at every several thousand cycles.

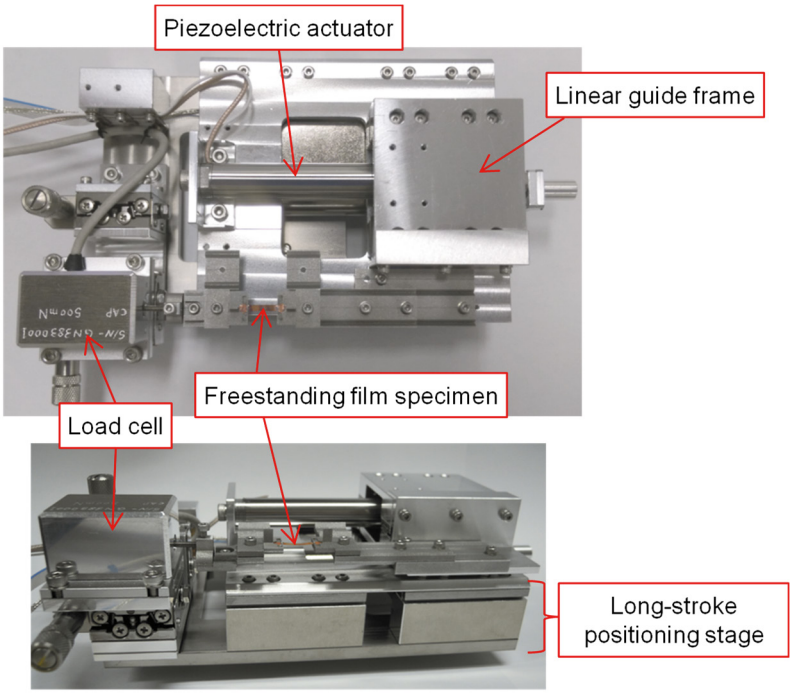

Fig. 3 *In situ* FESEM fatigue testing machine for freestanding film specimens.

3. Results and discussions

3.1. Capability of fatigue loading

Figure 4 shows applied stress to the film specimen during a fatigue crack propagation experiment in vacuum. The measured values of cyclic stress at a number of cycles $N \approx 1.0\times10^4$ is shown in Fig. 4(a) as an example. The correlation coefficient between the measured values and the target waveform (σ_{max} = 130 MPa, R = 0.1, f = 10 Hz) is 0.9998. Maximum and minimum stresses at every $N = 5.0 \times 10^2$ during the fatigue crack propagation experiment (up to $N = 2.24 \times 10^5$) are shown in Fig. 4(b). The maximum and minimum stresses in the experiment were 129.7 ± 0.3 MPa and 13.2 ± 0.3 MPa, respectively, indicating that the fatigue testing machine is capable to apply accurate cyclic stress to submicron-thick freestanding film specimens.

3.2. Fatigue crack propagation behavior

Figure 5 shows *in situ* FESEM observation images of fatigue crack propagation in vacuum at stress intensity factor range $\Delta K \approx 2.4$ MPam$^{1/2}$. Before applying cyclic load, a slip line was observed ahead of the notch root as shown in Fig. 5(a). By $N = 2.0 \times 10^3$ (Fig. 5(b)), fatigue damages such as intrusions/extrusions were observed ahead of the notch root. By $N = 5.0 \times 10^3$ (Fig. 5(c)), the range of fatigue damage formation expanded and the intrusions/extrusions grew larger. By $N = 9.0 \times 10^3$ (Fig. 5(d)), fatigue crack propagated from the initial notch root and through the intrusions/extrusions. Moreover, new intrusions/extrusions were formed ahead of the crack tip. The fatigue crack then propagated by the same manner: preceding intrusions/extrusions were formed ahead of the fatigue crack tip, and the fatigue crack then propagated preferentially through these intrusions/extrusions, as shown in Figs. 5(e) and (f). This fatigue crack propagation behavior is similar to that in the low-K_{max} region in air.

The mechanisms of fatigue crack propagation, however, transited as ΔK increased. At $N = 2.03 \times 10^5$ (Fig. 6(a)) ($\Delta K \approx 4.1$ MPam$^{1/2}$), intrusions/extrusions were not observed near the crack tip, and instead slip lines were formed ahead of the crack tip, indicating that the region ahead of the crack tip was plastically stretched. As shown in Fig.

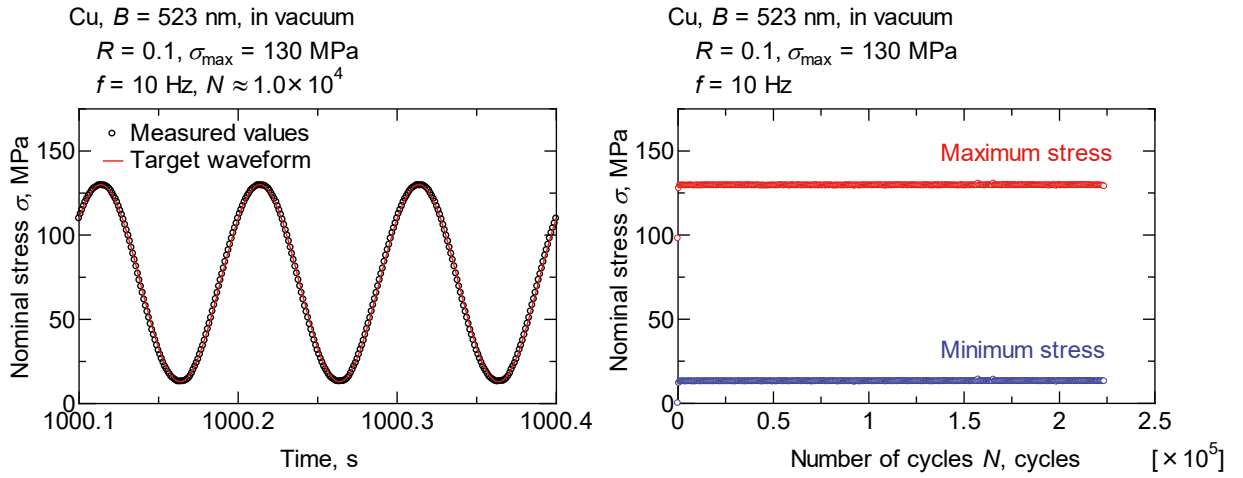

(a) Fatigue loading waveform at $N \approx 1.0 \times 10^4$ (b) Maximum and minimum stress at every 5.0×10^2 cycles

Fig. 4 Applied stress to the film specimen during fatigue crack propagation experiment in vacuum.

6(b) ($N = 2.04 \times 10^5$) and 6(c) ($N = 2.05 \times 10^5$), the fatigue crack propagated through these slip lines. The edges of the crack paths were plastically stretched, indicating that the fatigue crack propagation accompanied with necking deformation in the thickness direction, in other words, the fatigue crack propagated in tensile fracture mode. This fatigue crack propagation behavior is similar to that in the high-K_{max} region in air.

3.3. Effects of vacuum environment on fatigue crack propagation properties

Figure 7 shows crack length (a) vs. number of cycles (N) relationships obtained by the experiments in both air and vacuum environments under the same condition ($\sigma_{max} = 130$ MPa, $R = 0.1$, $f = 10$ Hz and the initial notch length of ~100 μm). In both environments, the fatigue crack stably propagated. The fatigue crack propagation gradually

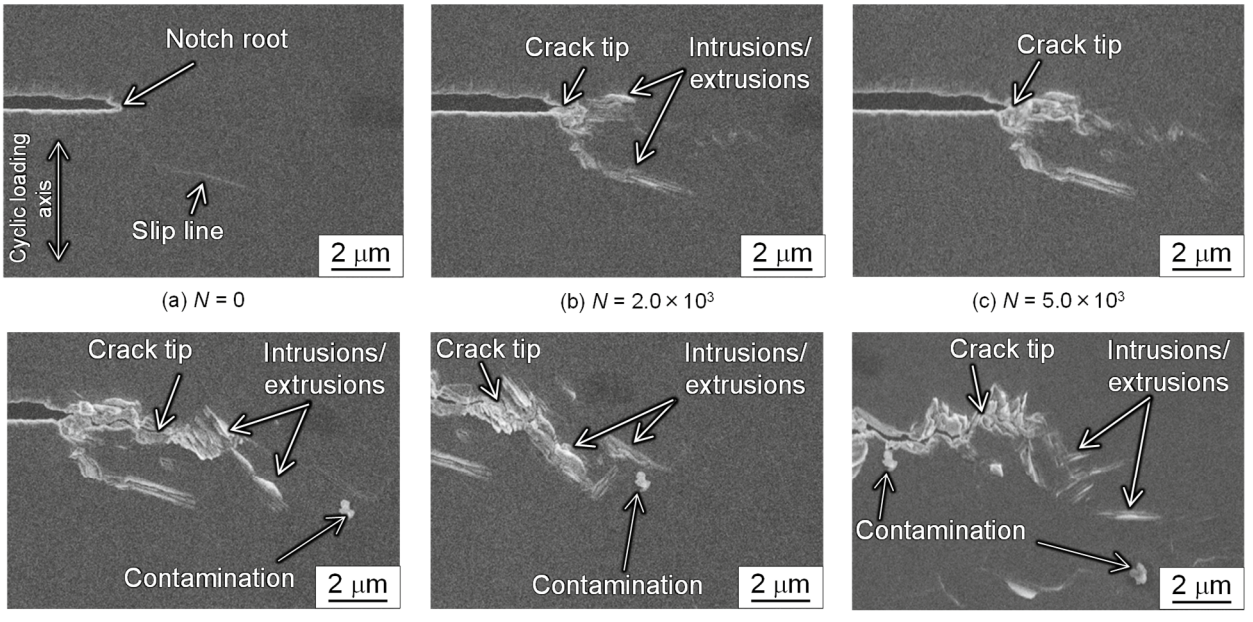

(a) $N = 0$ (b) $N = 2.0 \times 10^3$ (c) $N = 5.0 \times 10^3$

(d) $N = 9.0 \times 10^3$ (e) $N = 1.7 \times 10^4$ (f) $N = 3.0 \times 10^4$

Fig. 5 Sequential FESEM snapshots of fatigue crack propagation at $\Delta K \approx 2.4$ MPam$^{1/2}$.

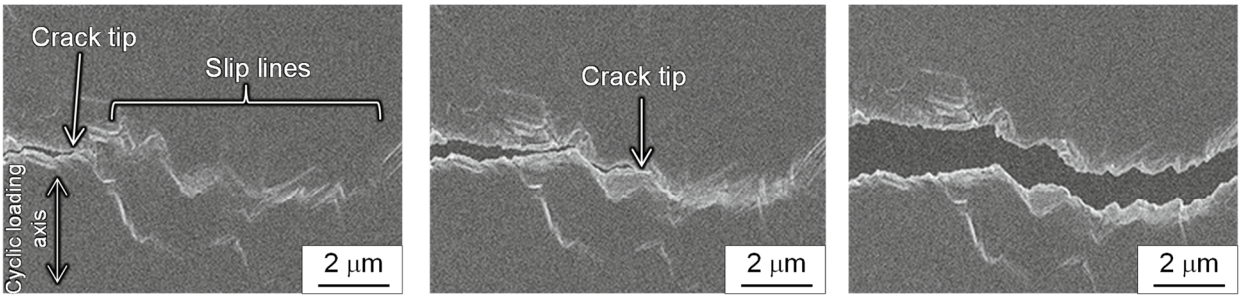

(a) $N = 2.03 \times 10^5$ (b) $N = 2.04 \times 10^5$ (c) $N = 2.05 \times 10^5$

Fig. 6 Sequential FESEM snapshots of fatigue crack propagation in vacuum at $\Delta K \approx 4.1$–4.5 MPam$^{1/2}$.

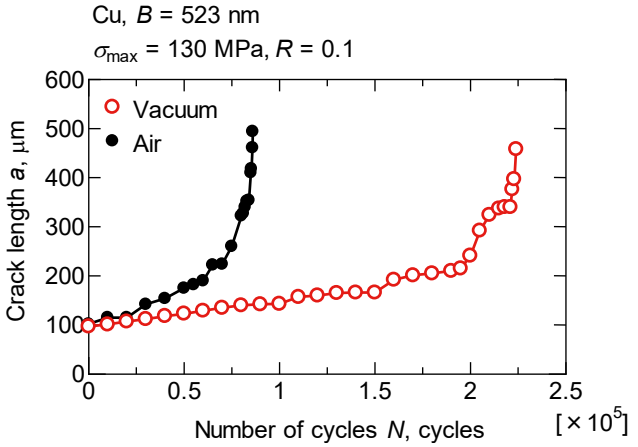

Fig. 7 Effects of vacuum environment on a vs. N relationship under the same condition.

accelerated and then the specimens were finally fractured unstably. N at unstable fracture in vacuum is ~2.6 times longer than that in air, indicating that fatigue crack propagation was decelerated due to the vacuum environment.

Fatigue crack propagation rate (da/dN) vs. stress intensity factor range (ΔK) relationships in air and vacuum environments are shown in Fig. 8. da/dN in both environments increased as ΔK increased. Focused on the vacuum effect, da/dN in both environments are roughly within a narrow band in $\Delta K \gtrsim 4$–5 MPam$^{1/2}$. In contrast, da/dN in vacuum was smaller than that in air in the region of $\Delta K \lesssim 4$–5 MPam$^{1/2}$. This result indicates that vacuum environments decelerated the fatigue crack propagation in the region of $\Delta K \lesssim 4$–5 MPam$^{1/2}$.

3.4. Fracture surface morphologies

Figure 9 shows FESEM micrographs of the fracture surfaces (a) fatigued in air and (b) in vacuum in the region of $\Delta K \lesssim 4$–5 MPam$^{1/2}$. Relatively flat surfaces and the surface steps with a sharp edge were often observed on the fracture surface fatigued in air, as shown in Fig. 9(a). In contrast, flat surfaces were rarely observed and blunt fracture surfaces with fine roughness were observed on the surface fatigued in vacuum, as shown in Fig. 9(b). These differences on the fracture surface morphologies suggest the dependence of the environments on the fatigue damage formation mechanisms. In ambient air, fresh surface oxidation occurred during cyclic slip deformation process. In this condition, rewelding was inhibited and irreversible cyclic slip deformation would accelerate the fatigue crack propagation or intrusions/extrusions formation. In contrast, the suppression of fresh surface oxidation occurs in vacuum environments, leading to the reversible slip deformation and rewelding of fracture surfaces. In this condition, the fatigue crack propagation or intrusions/extrusions formation would be decelerated. These environmental effects would cause smaller da/dN in vacuum than in air.

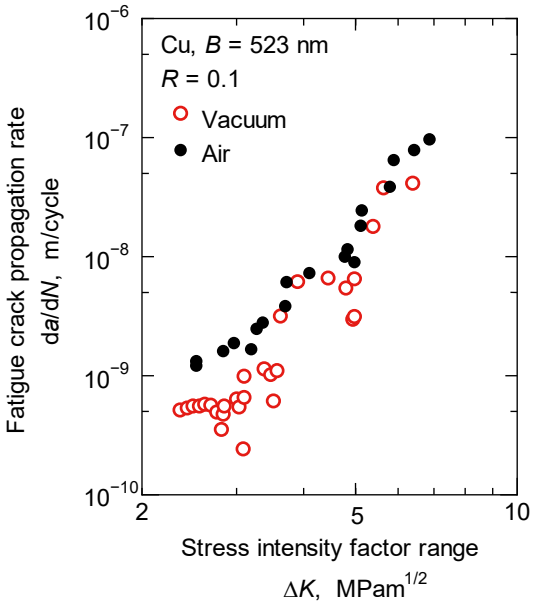

Fig. 8 Comparison of da/dN vs. ΔK relationship between in air and vacuum.

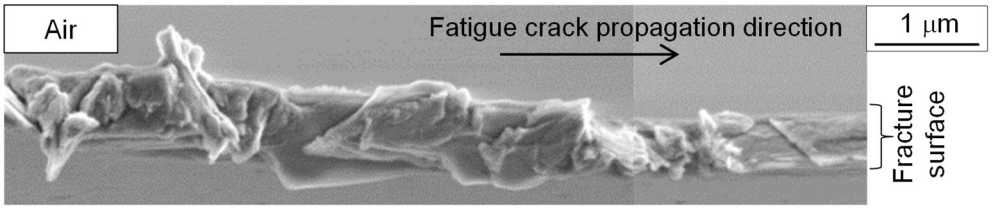

(a) Fracture surface fatigued in air

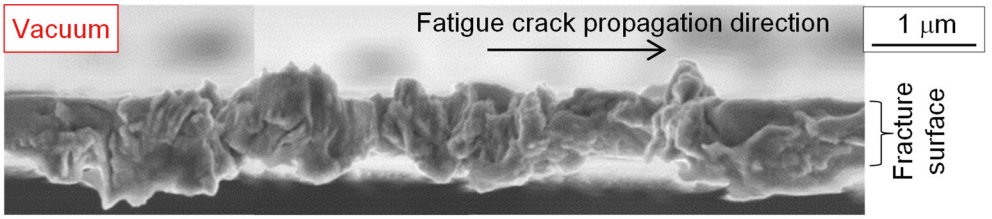

(b) Fracture surface fatigued in vacuum

Fig. 9 FESEM micrographs of fracture surfaces fatigued in air and vacuum in the region of $\Delta K \lesssim$ 4–5 MPam$^{1/2}$.

4. Conclusions

The effects of vacuum environment on fatigue crack propagation properties were investigated in approximately 500 nm thick freestanding Cu films at R of 0.1. Fatigue crack propagation experiments were conducted in both air and vacuum environments, and the fracture surface morphologies were compared. The results are summarized as follows:

- We developed an *in situ* FESEM fatigue testing machine for fatigue crack propagation of submicron-thick freestanding film specimens in ambient air and vacuum. The machine is capable to apply accurate cyclic stress to submicron-thick freestanding film specimens.

- *In situ* FESEM observations of fatigue crack propagation revealed that the fatigue crack in vacuum propagated by similar mechanisms in air: in the lower ΔK, preceding intrusions/extrusions were formed ahead of the crack tip, and the fatigue crack then propagated preferentially through these intrusions/extrusions. In the higher ΔK, the fatigue crack propagated in tensile fracture mode.
- Crack length (a) vs. number of cycles (N) relationships, and fatigue crack propagation rate ($\mathrm{d}a/\mathrm{d}N$) vs. stress intensity factor range (ΔK) relationships in air and vacuum environments indicate that the vacuum environment decelerated the fatigue crack propagation in the region of $\Delta K \lesssim 4$–5 $\mathrm{MPam}^{1/2}$. Flat surfaces and the surface steps with a sharp edge were observed on the fracture surface fatigued in air, whereas blunt surfaces with fine roughness were observed on the fracture surface fatigued in vacuum, suggesting that the mechanisms of fatigue damage formation depends on the environments.

Acknowledgements

This work was supported by JSPS KAKENHI Grant Numbers 23246026 and 26220901.

References

Hudson, CM., Seward, SK., 1976. A literature review and inventory of the effects of environment on the fatigue behavior of metals. Engineering Fracture Mechanics 8, 315-329.

Ishii H., Weertman, J., 1969. The effect of air pressure on the rate of fatigue crack growth. Scripta Metallurgica 3, 229-232.

Kondo, T., Imaoka, T., Hirakata, H., Sakihara, M., Minoshima, K., 2013. Effects of stress ratio on fatigue crack propagation properties of submicron-thick free-standing copper films. Acta Materialia 61, 6310-6327.

Murakami, Y. (Editor), 1986. in "*Stress Intensity Factors Handbook*", Pergamon Press, Oxford, p. 9.

Pelloux, RMN., 1970. Crack extension by alternating shear. Engineering Fracture Mechanics 1, 697-704.